ARQII Publication
http://arqiipubl.com/ams
APPLICATIONS OF
MODELLING AND SIMULATION
eISSN 2600-8084
VOL 4, 2020, 280-289

Forecasting of Erosion Rate in Tee-Junctions for Liquid-Solid Flow via Computational Fluid Dynamics (CFD)

A. Z. A. A. Jashmady[1], A. Supee[1,2*], M. D. M. Samsudin[1,2] and N. B. Haladin[3]

[1]School of Chemical and Energy Engineering, Faculty of Engineering, Universiti Teknologi Malaysia, Malaysia
[2]Energy Management Group, School of Chemical and Energy Engineering, Faculty of Engineering, Universiti Teknologi Malaysia, Malaysia
[3]Language Academy, Universiti Teknologi Malaysia, Malaysia

[*]Corresponding author: aizuddin@utm.my

Submitted 02 July 2020, Revised 13 August 2020, Accepted 18 August 2020.

Abstract: This work intends to forecast the influence of parameters such as particles size, stream velocities and tee-junctions diameter towards an erosion rate of a tee-junction in light crude oil ($C_{19}H_{30}$)-solid (sand) flow. A commercially available ANSYS Fluent 2020 R1 (Academic Version)-computational fluid dynamics (CFD) was used to numerically predict the erosion rate in tee-junctions. Three different models were applied in CFD approach named as continuous flow modeling, Lagrangian particle tracking and empirical erosion equation. The ranges of simulated parameters include 100-500 µm particles size, 3-7 m/s stream velocities and 0.0762-0.1778 m tee-junctions diameter. The location of maximum erosion rate for all the simulated parameters are found to be at the mid-section of the tee-junction. The maximum erosion rate is reduced with the increasing of the particles size while increased with the increasing of the stream velocities. However, there is no correlation found for the maximum erosion rate (increased or decreased) with the tee-junctions diameter.

Keywords: Computational fluid dynamics (CFD); Light crude oil-solid flow; Maximum erosion rate and location; Particles size and stream velocities; Tee-junctions diameter.

1. INTRODUCTION

Transportation of fluid is not something new in the oil and gas industry. From the downstream to the upstream, almost all of the processes involved fluid transportation. One of the most common fluid transportation in the oil and gas industries is fluids transportation with entrained solid particles or known as liquid-solid flow. Normally, the fluids which are extracted from the reservoir and transported to the nearest processing plants will carry together the solid particles across the streamlines of the pipeline. Complex pipeline with numerous technologies from all over the world implemented in order to boost the efficiency of an industry in handling or managing these types of flows. This includes the transportation of fluids through piping system with several fittings such as elbows, tee-junctions, reducers, expanders, bends, couplings, valves, etc. as well as other fluids handling equipment such as pumps, compressors, heat exchangers, heaters, and boilers. The movement of fluids in the pipeline system is a dynamic process whereby it involved changes in velocity as well as the directions. Changes in flow direction creates solid particle's inertia due to deviation from the streamlines of the carrying fluids, and thus, resulting in particles impingement on the wall of the components in pipeline systems [1]. This phenomenon is called as erosions as it involves metal removal process caused by solid particles impact [2-4]. The erosion damage may cause pipeline systems failure which eventually leads to loss of cost and productivity, and requirement to substitute damaged components. Thus, it is essential to reduce the solid particles erosion effects as much as possible by possessing better comprehension in the physics of particulate flow.

Tee-junction is one of the susceptible to erosion environment in a pipeline system. Some researchers have elected tee-junction as the crucial component in pipeline system for their research in order to obtain a clearer insight of erosion phenomenon involved. Numerous method of erosion prediction in tee-junctions were applied by them such as by experimental [5-7], empirical correlations and mechanistic models [5], and the computational fluid dynamics (CFD) [8-9]. Chen *et al.* [10] studied the effects of the particle rebound model on the particle trajectories as well as erosion pattern in the tee using both the experimental and CFD studies. They found that the maximum erosion predicted by the stochastic particle rebound model occurred on the end surface of the tee. Meanwhile, in their different works, they conclude that, the stream velocity affects the erosion rate and this is due to the multiple impingements of one particle. Both the simulations and experimental results exhibit that, significant erosion occurred at the end, side and corner regions of the tees using the air flow of 45.72 m/s and the-tee

diameter of 0.0254 m [5, 10]. However, different location of maximum erosion rate was observed when they changed the airflows to the waterflows. More particles deviated from the main streamlines and impinge the tee at the joint corner area. This is caused by the high drag and inertia forces exerted on the particles by water. Erosion in tee-junctions is a complicated process and depends on a various factor such as the properties of fluid and particles, the production rate for the produced fluid and particles, concentration of particles, diameter of tee-junctions and as well as the particles size. An increment in particle mass loading by a factor of 10 results in increased in erosion magnitude (approximately one order of magnitude) in tee [11]. Higher stream velocity which yield greater particles momentum will cause in higher erosion rate [12]. Meanwhile, the erosion rate decreases as the diameter of tee-junctions increase. This is due to the velocity of small particles within the region of the tee dramatically decreases, which then significantly reduces the penetration rate [13].

Despite a lot of work reported on the erosion prediction for the tee-junctions component in pipeline system [5-13], yet, there is still inadequate information on the forecasting based on the stream velocity less than 10 m/s. Apart from that, current work applied different fluid type which is light crude oil ($C_{19}H_{30}$) as a liquid as compared to those reported works. In this work, a commercially available ANSYS Fluent 2020 R1 (Academic Version)-CFD was used to numerically predict the erosion rate in tee-junctions for a broad range of liquid/solid particles flow conditions. Similar to our previous works for elbows [14], the erosion rate for the simulated tees was analyzed under three different parameters namely particles size (100 to 500 μm), the tee-junctions diameter (0.0762 m to 0.1778 m) and stream velocity (3 to 7 m/s).

2. SIMULATION

The erosion forecasting was simulated using three different models called as continuous flow modeling, particle tracking, and application of empirical erosion equation [14]. Continuous flow modeling was commenced by producing the computational grid and proceeded with specifying the solution preferences such as the conditions of inlet and boundary, the turbulence model, and the operating conditions. Particles were introduced into the flow after obtaining a flow solution at tee-junctions. Lagrangian particles tracking method was employed to numerically determine the trajectories of droplets and solid particles through the flow. The trajectory of particles was determined by taking into consideration the external forces imposed on the particles. Based on the information on particles impingement on the wall of tees, the mass loss or suitably called as erosion rate, caused by that impingement, was determined by empirical erosion equation. Prior to simulation work, we performed the manual calculation of Reynolds number (Re_f) for fluid system (light crude oil: $C_{19}H_{30}$) using an equation of:

$$Re_f = \frac{\rho_f V_f \phi_{tee-junctions}}{\mu_f} \quad (1)$$

All the values of Re_f for our simulated fluid system are prevails within the turbulence range (Re > 4000). This verified our assumption of turbulence flow inside the tee-junctions and justify the suitability of Renormalization group (RNG) k-epsilon model (turbulence modeling) opted in this CFD simulation. All the parameters and assumptions involved in CFD forecasting modeling as well as manual calculation of Reynolds number (prior to simulation work for fluid system) are listed in Table 1.

Table 1. Parameters and assumptions set in CFD simulator and manual calculation of Reynolds number (prior to simulation work for fluid system)

Parameter	Explanation
Turbulence modeling	• Renormalization group (RNG) k-epsilon model
Fluid system	• Light crude oil: $C_{19}H_{30}$ • Density: 960 kg/m^3 • Viscosity: 0.048 kg/m.s
Tee-junctions system	• Material: carbon steel • Density: 7850 kg/m^3
Operating temperature	• Room temperature: 25 °C
Particles system	• Material: sand • Number of particles: 10000 • Shape: spherical • Density: 2600 kg/m^3 [15-16]
Assumptions	• The flow inside the tee-junctions are turbulence flow • Incompressible and constant properties of fluid • Spherical shape of particles in the particle tracking method • Interaction between solid particles and the effect of particles motion on the fluid flow are small and can be neglected

	Conditions	Manipulated parameters	Stream (fluid and particles) velocity (m/s)	Tee-junctions diameter (m)	Size of particles (μm)	Reynolds number calculation for fluid system (prior to simulation work)
Simulated flow conditions	1	Size of particles (μm): 100 200 300 400 500	4	0.1016	-	8128
	2	Stream velocities (m/s): 3 4 5 6 7	-	0.1016	200	6096 8128 10160 12192 14224
	3	Tee-junctions diameter (m): 0.0762 0.1016 0.1270 0.1524 0.1778	4	-	200	6096 8128 10160 12192 14224

2.1 The Continuous Phase Model

The conservation equations for mass (continuity) and momentum in addition to the equations representing the turbulence model were used to forecast the flow pattern of the continuous flow phase and the said equations are as followed [17-18]:

Equation for the mass (continuity) conservation:

$$\left(\frac{\partial}{\partial x_i}\right)(\rho \bar{U}_i) + \left(\frac{\partial}{\partial x_j}\right)(\rho \bar{U}_j) + \left(\frac{\partial}{\partial x_k}\right)(\rho \bar{U}_k) = 0 \tag{2}$$

Equation for the momentum conservation in *i*-direction:

$$\left(\frac{\partial}{\partial x_i}\right)(\rho \bar{U}_i \bar{U}_i) + \left(\frac{\partial}{\partial x_j}\right)(\rho \bar{U}_j \bar{U}_i) + \left(\frac{\partial}{\partial x_k}\right)(\rho \bar{U}_k \bar{U}_i) = -\left(\frac{\partial \bar{P}}{\partial x_i}\right) + \mu_{eff}\left(\frac{\partial^2 \bar{U}_i}{\partial {x_i}^2} + \frac{\partial^2 \bar{U}_i}{\partial {x_j}^2} + \frac{\partial^2 \bar{U}_i}{\partial {x_k}^2}\right) - \left(\frac{\partial}{\partial x_i}\right)(\rho \overline{u_i u_i}) \tag{3}$$

Equation for the momentum conservation in *j*-direction:

$$\left(\frac{\partial}{\partial x_i}\right)(\rho \bar{U}_i \bar{U}_j) + \left(\frac{\partial}{\partial x_j}\right)(\rho \bar{U}_j \bar{U}_j) + \left(\frac{\partial}{\partial x_k}\right)(\rho \bar{U}_k \bar{U}_j) = -\left(\frac{\partial \bar{P}}{\partial x_j}\right) + \mu_{eff}\left(\frac{\partial^2 \bar{U}_j}{\partial {x_i}^2} + \frac{\partial^2 \bar{U}_j}{\partial {x_j}^2} + \frac{\partial^2 \bar{U}_j}{\partial {x_k}^2}\right) - \left(\frac{\partial}{\partial x_i}\right)(\rho \overline{u_j u_i}) \tag{4}$$

Equation for the momentum conservation in *k*-direction:

$$\left(\frac{\partial}{\partial x_i}\right)(\rho \bar{U}_i \bar{U}_k) + \left(\frac{\partial}{\partial x_j}\right)(\rho \bar{U}_j \bar{U}_k) + \left(\frac{\partial}{\partial x_k}\right)(\rho \bar{U}_k \bar{U}_k) = -\left(\frac{\partial \bar{P}}{\partial x_k}\right) + \mu_{eff}\left(\frac{\partial^2 \bar{U}_k}{\partial {x_i}^2} + \frac{\partial^2 \bar{U}_k}{\partial {x_j}^2} + \frac{\partial^2 \bar{U}_k}{\partial {x_k}^2}\right) - \left(\frac{\partial}{\partial x_i}\right)(\rho \overline{u_k u_i}) \tag{5}$$

The momentum equations have the term $-\left(\frac{\partial}{\partial x_i}\right)(\rho \overline{u_j u_i})$ given in compact stress tensor notation. This term represents the effect that turbulence motion has on the time average known as Reynold's stresses which are high frequency fluctuating components of velocity. In *i*-direction:

$$\left(\frac{\partial}{\partial x_i}\right)(\rho \overline{u_i u_i}) \text{ expands to } -\left(\frac{\partial}{\partial x_i}\right)(\rho \overline{u_i u_i}) + \left(\frac{\partial}{\partial x_i}\right)(\rho \overline{u_j u_i}) + \left(\frac{\partial}{\partial x_i}\right)(\rho \overline{u_k u_i}) \tag{6}$$

where *P* in momentum equations (Equations (3) to (5)) is the static pressure and the stresses in tensor notation can be related as follows:

$$\rho\overline{u_j u_i} = \mu_T \left(\frac{\partial \bar{U}_j}{\partial x_i} + \frac{\partial \bar{U}_i}{\partial x_j}\right) - \frac{2}{3}\rho k \delta_{ji} \tag{7}$$

The δ_{ji} is equal to 0 if $i \neq j$, equals to 1 if $i = j$ and effective viscosity, $\mu_{eff} = \mu_T + \mu$ where δ_{ji} is Kronecker delta and turbulence viscosity, μ_T is given by:

$$\mu_T = \rho\, C_\mu (k^2/\varepsilon) \tag{8}$$

with $C_\mu = 0.0845$.

Equation (8) was acquired by solving both following turbulence modeling equations (Equations (9) and (10)). The kinetic energy of turbulence:

$$\left(\frac{\partial}{\partial x_i}\right)(\rho \bar{U}_i k) = \left(\frac{\partial}{\partial x_j}\right)\left[\left(\frac{\mu_{eff}}{\sigma_k}\right)\left(\frac{\partial k}{\partial x_j}\right)\right] + G_k - \rho\varepsilon \tag{9}$$

The dissipation rate of kinetic energy in turbulence:

$$\left(\frac{\partial}{\partial x_i}\right)(\rho \bar{U}_i \varepsilon) = \left(\frac{\partial}{\partial x_j}\right)\left[\left(\frac{\mu_{eff}}{\sigma_\varepsilon}\right)\left(\frac{\partial \varepsilon}{\partial x_j}\right)\right] + C_{\varepsilon 1} G_k \left(\frac{\varepsilon}{k}\right) - (C_{\varepsilon 2} + C_{\varepsilon 3})\rho\left(\frac{\varepsilon^2}{k}\right) \tag{10}$$

where G_k denotes the generation of turbulent kinetic energy owing to the mean velocity gradients and it is given by:

$$G_k = -\rho\overline{u_j u_i}\left(\frac{\partial \bar{U}_j}{\partial x_i}\right) \tag{11}$$

The quantities of σ_k and σ_ε are the effective Prandtl numbers for k and ε respectively and $C_{\varepsilon 3}$ as a function of the k/ε are given by previous researchers [19]. The model values for $C_{\varepsilon 1}$ and $C_{\varepsilon 2}$ is 1.42 and 1.68.

2.2 Particle Tracking

Generally, earlier researchers utilize Eulerian and Lagrangian methods to numerically determine the trajectories of droplets and solid particles through the flow [20-22]. Durst *et al.* [20] compared both the methods in forecasting particulate two phase flows and deduced that Lagaragian method has some distinct advantages for forecasting the particulate flows with substantial acceleration. Moreover, it could also handle particulate two phase flows comprising of poly dispersed particle size distribution. For this work, Lagrangian particles tracking method has been opted in determining the velocity of the particles as well as its trajectory before any impact towards tee-junctions wall. Solid surface erosion and determination of particle trajectory during the motion of following impact have been estimated by using this impact velocity data. Based on the well-known Newton's second law, governing equations of particles motion suggested by Clift *et al.* [23] have been applied in this work and it is described as follow:

$$m_p\left(\frac{dV_p}{dt}\right) = F_D + F_P + F_B + F_A \tag{12}$$

Equation (12) contains of drag force, pressure gradient force, buoyancy force and added mass force:

$$\text{Drag force } (F_D) = C_D \rho_f\, \pi \frac{\phi_p^2 |V_f - V_p|(V_f - V_p)}{8} \tag{13}$$

where C_D is the drag coefficient and it is given by:

$$C_D = \left(\frac{24}{Re_s}\right)(1 + 0.15 Re_s^{0.687}) \tag{14}$$

and particle relative Reynolds number Re_s is defined by:

$$Re_s = \frac{[\rho_f |V_p - V_f| \phi_p]}{\mu_f} \tag{15}$$

Pressure gradient force:

$$F_P = \pi \phi_p^3 \nabla \frac{P}{4} \tag{16}$$

Buoyancy force:

$$F_B = \pi \frac{\phi_p^3 (\rho_p - \rho_f) g}{6} \tag{17}$$

Added mass force:

$$F_A = -\frac{\pi \phi_p^3 \rho_p dV_p}{12dt} \tag{18}$$

2.3 Erosion Rate (ER) Prediction

The model accessible in the ANSYS Fluent 2020 R1 (Academic Version)-CFD for the calculation of the *ER* have been selected by considering the parameters such as mass flow rate of the particles ($\dot{m}_p$), function of particles diameter ($C(\phi_p)$), function of the impact angle ($f(\alpha)$), relative particles velocity (V_p), function of relative particles velocity ($b(V_p)$) and the area of the wall face where the particles strikes the boundary (A_{face}). The empirical erosion equation used is as followed:

$$ER = \sum_{i=1}^{Nparticle} \dot{m}_p \frac{C(\phi_p) f(\alpha) V_p^{b(Vp)}}{A_{face}} \tag{19}$$

3. RESULTS AND DISCUSSION

Three parameters were altered to demonstrate their influence on the erosion rate of the tee-junctions named as particles size (100-500 µm), stream velocity (3-7 m/s) and tee-junctions diameter (0.0762-0.1778 m). Throughout the simulation, another two parameters were set to constant for each simulated flow conditions as stated in Table 1. Maximum erosion rate graphs and visual illustration of erosion rate surface contours have been used to elucidates the influences of flow conditions viz. size of particles, stream velocity and tee-junctions diameter on erosion rate of the tee-junctions.

3.1 Influences of Particles Size towards Tee-Junctions Erosion Rate using the Flow Condition 1

Erosion rate surface contours for the particles size ranging from 100 to 500 µm are shown in Figure 1 to Figure 5. At glance, similar patterns observed for the maximum erosion rate when the size of particles varied whereby the location of these maximum erosion rate occurred at the mid-section of the tee-junctions. The justification for the similarity possibly caused by slight density difference for the carrier fluid at temperature of 25 °C (density of water: 997 kg/m^3; density of light crude oil: 960 kg/m^3). Thus, the drag force exerted on particles by carrier fluid more less have the same magnitude for both the water and light crude oil system. After multiple impingements at the mid-section and horizontal area (two outlet) of the tee-junctions, the deviated particles then follow the streamline again.

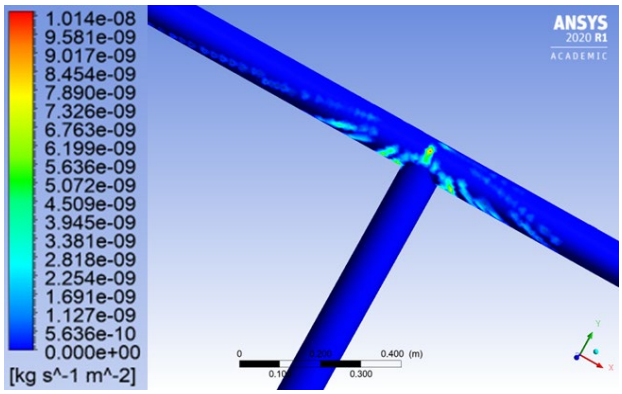

Figure 1. Erosion rate (kg/m^2.s) surface contour for 100 µm particles size

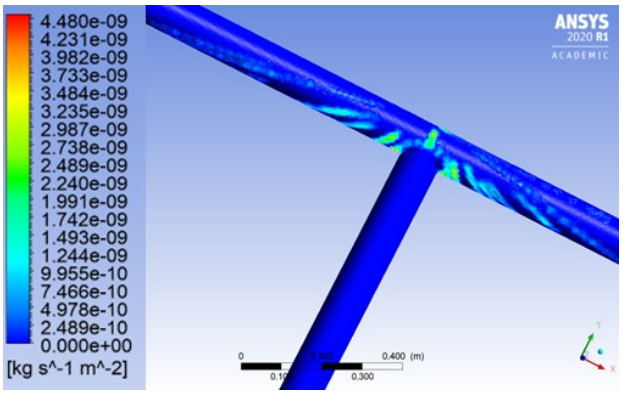

Figure 2. Erosion rate (kg/m^2.s) surface contour for 200 µm particles size

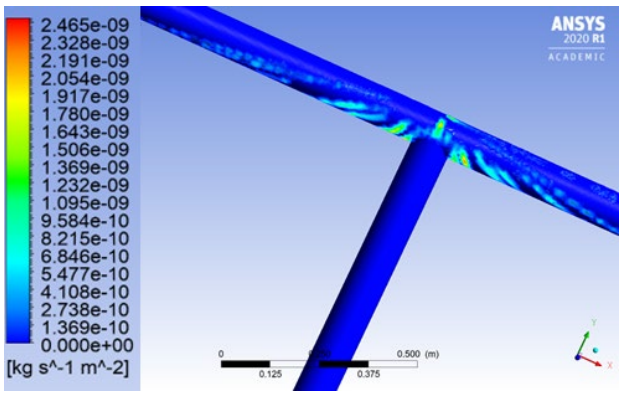

Figure 3. Erosion rate (kg/m^2.s) surface contour for 300 µm particles size

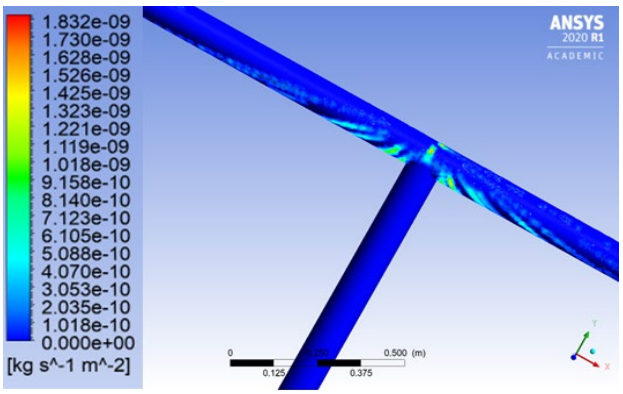

Figure 4. Erosion rate (kg/m^2.s) surface contour for 400 µm particles size

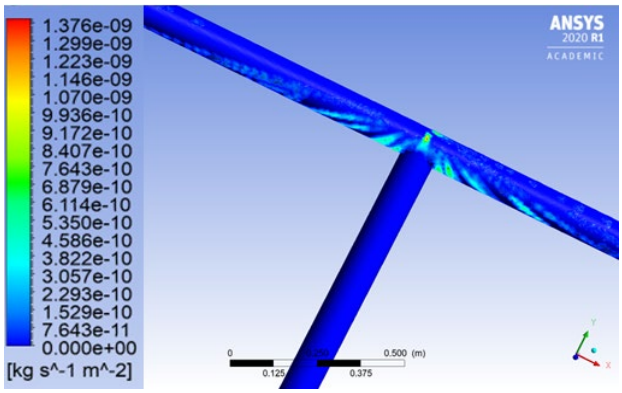

Figure 5. Erosion rate (kg/m^2.s) surface contour for 500 µm particles size

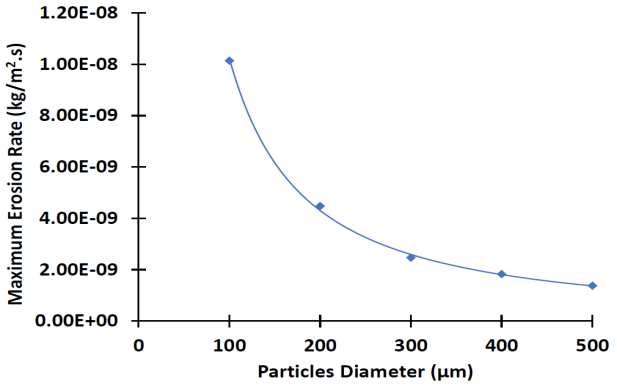

Figure 6. Maximum erosion rate (kg/m^2.s) versus particles (sand) diameter (µm)

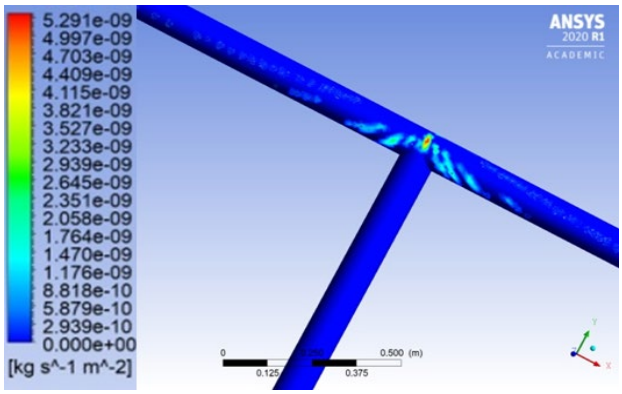

Figure 7. Erosion rate (kg/m^2.s) surface contour for 3 m/s stream velocity

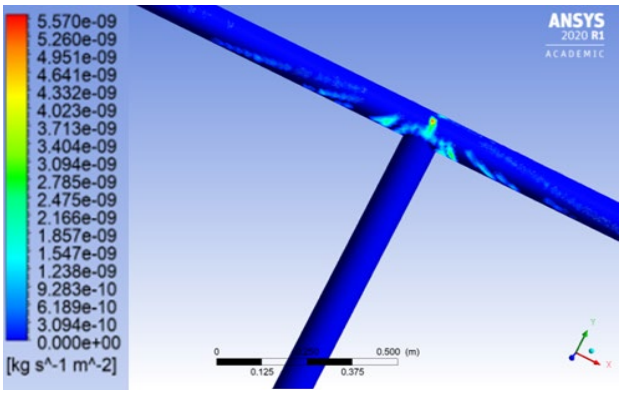

Figure 8. Erosion rate (kg/m^2.s) surface contour for 4 m/s stream velocity

Figure 6 depicts the maximum erosion rate occurred for the tee-junctions with flow condition 1. Maximum erosion rate was affected by the size of particles and increased in particles size will lead to the decrease in maximum erosion rate. Similar pattern was also obtained by previous researcher [24]. Particle size of 100 µm results in the highest maximum erosion rate which is 1.08×10^{-8} kg/m^2.s. This is due to light weight of the particle which results in rapid indentation on the wall of the tee-junctions. The rapid the indentation, the greater the amount of material removed (higher maximum erosion rate). However, the greater the size of the particle results in further dispersion of the particles in tee junction due to the bigger mass of particle results in greater inertia. For this work, the size of particles were set to the range of 100 to 500 µm since this is regular size found in oil and gas industry [25].

3.2. Influences of Stream Velocity towards Tee-Junctions Erosion Rate using the Flow Condition 2

Figure 7 to Figure 11 illustrate erosion rate surface contours for the tee-junctions using different stream velocities. All the velocities exhibited similarity in term of the location of the maximum erosion rate which occurred at the mid-section of the tee-junctions. This is possibly because of gravity effects as the inlet flow moves in vertical direction of the tee-junctions. In horizontal area of the tee-junctions (mid-section to both outlet), the gravity effects are insignificant. In vertical area of the tee-junctions (inlet), the flow in opposition to the gravity direction and therefore, the particles tend to impinge at the mid-section of the tee-junctions. Erosion severity is stream velocity dependent whereby an increased in stream velocity resulted in increase in erosion severity. The momentum and inertia of the particles and fluid will increase as the stream velocity increase and as a result, the collision between particles and the wall of the tee-junctions also will increase. This statement is verified by Figure 11 whereby high stream velocity of 7 m/s results in severe erosion rate surface contours compared to other stream velocities.

Further graphical illustration on the severity values of the erosion rate caused by the stream velocities is shown in Figure 12. Maximum erosion rate was tremendously increased from 5.29×10^{-9} kg/m^2.s to 1.23×10^{-8} kg/m^2.s with the changes in stream velocity from 3 m/s to 7 m/s. The pattern obtained also alike with previous reported works [10, 17].

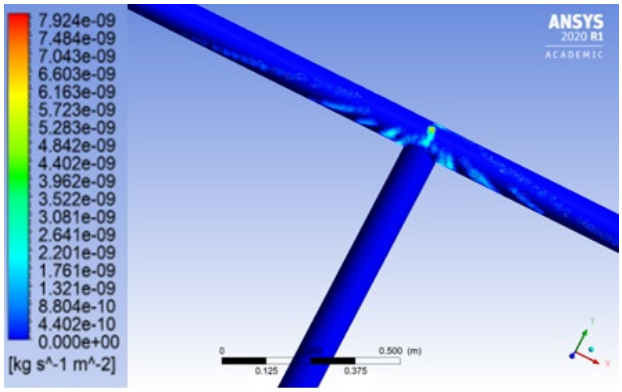

Figure 9. Erosion rate (kg/m^2.s) surface contour for 5 m/s stream velocity

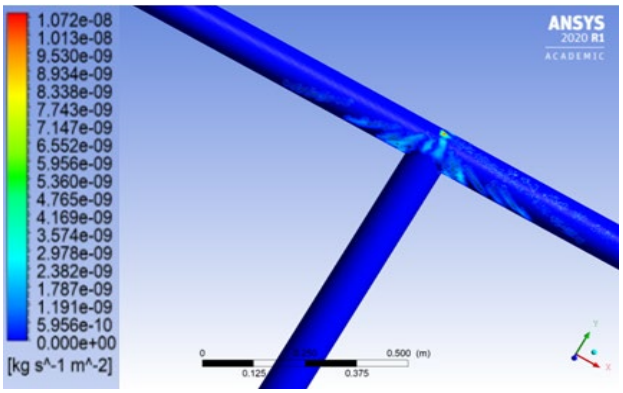

Figure 10. Erosion rate (kg/m^2.s) surface contour for 6 m/s stream velocity

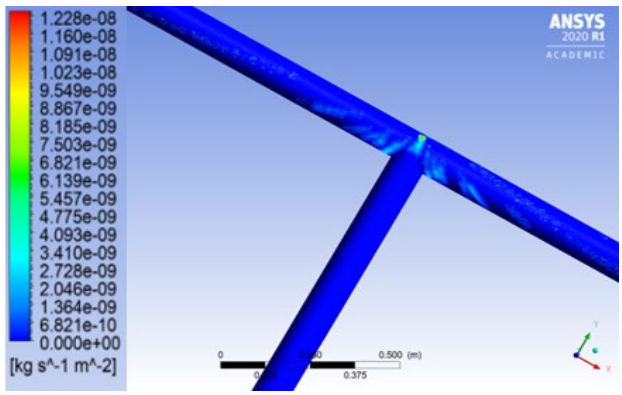

Figure 11. Erosion rate (kg/m^2.s) surface contour for 7 m/s stream velocity

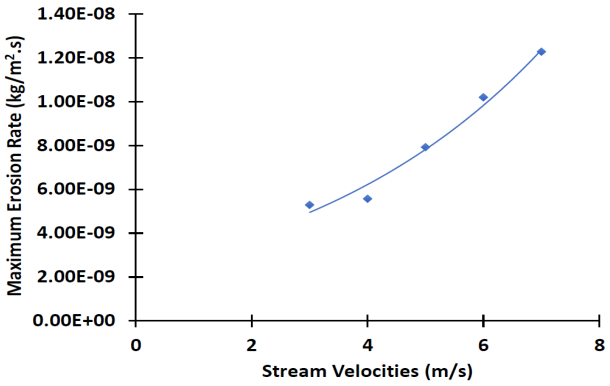

Figure 12. Maximum erosion rate (kg/m^2.s) versus stream velocities (m/s)

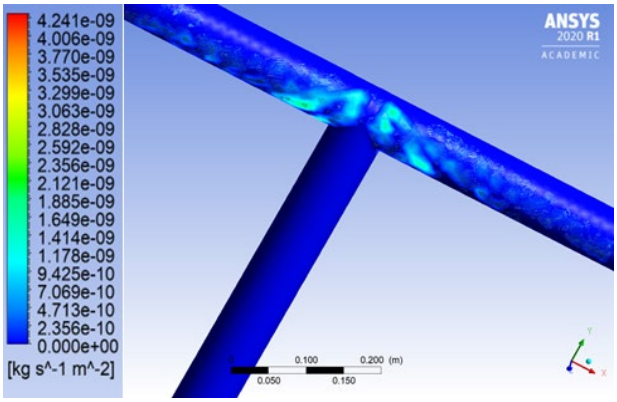

Figure 13. Erosion rate surface contour (kg/m^2.s) for 0.0762 m tee-junctions diameter

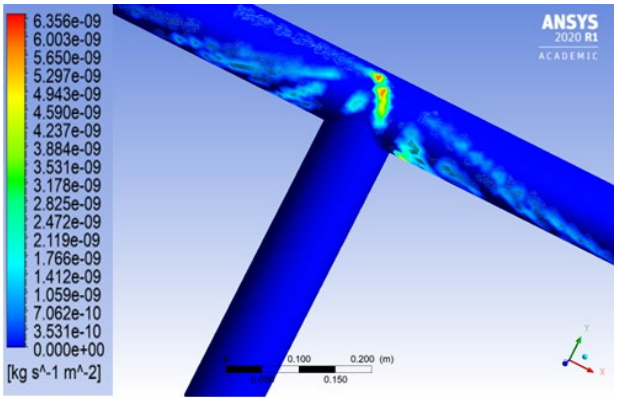

Figure 14. Erosion rate surface contour (kg/m^2.s) for 0.1016 m tee-junctions diameter

3.3. Influences of Tee-Junctions Diameter towards Tee-Junctions Erosion Rate using the Flow Condition 3

Erosion rate surface contours for various diameter of tee-junctions are depicted in Figure 13 to Figure 17. Similar patterns produced as the effects of stream velocity where maximum erosion rate occurred at the mid-section of tee-junctions. Based on the simulation, 0.1524 m diameter recorded the highest maximum erosion rate in tee-junctions. The plot of maximum erosion rate versus tee-junctions diameter is depicted in Figure 18. In flow condition 3, there was no specific pattern observed (increased or decreased) for the maximum erosion rate with increased diameter of the tee-junction. In previous work, the tee diameter used were from 0.4 m to 0.6 m [13]. Increased in the diameter of those tee results in decreased erosion. They also conclude that the erosion rate is independent to the tee diameter provided the flows involved particles size greater than 100 µm. Their findings matched our flow condition 3 where the maximum erosion rate is independent to tee-junctions diameter as the particle size used in flow condition 3 was 200 µm.

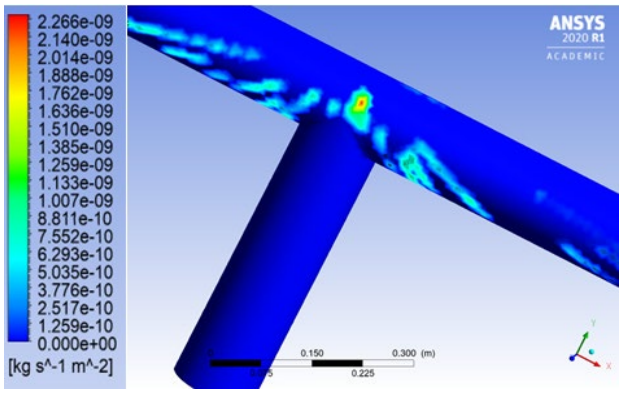

Figure 15. Erosion rate surface contour (kg/m^2.s) for 0.1270 m tee-junctions diameter

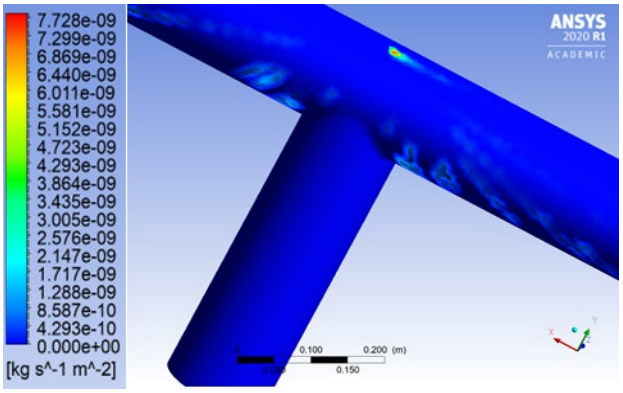

Figure 16. Erosion rate surface contour (kg/m^2.s) for 0.1524 m tee-junctions diameter

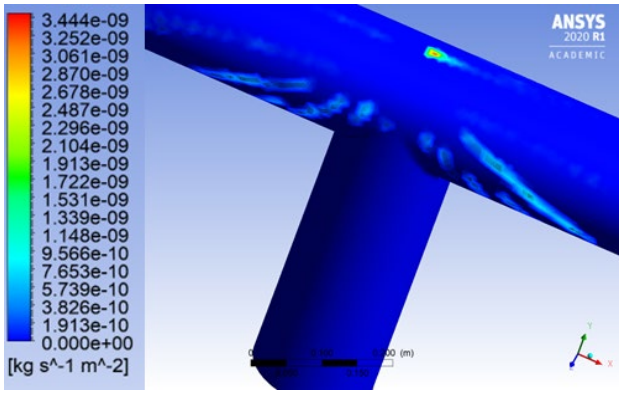

Figure 17. Erosion rate surface contour (kg/m^2.s) for 0.1778 m tee-junctions diameter

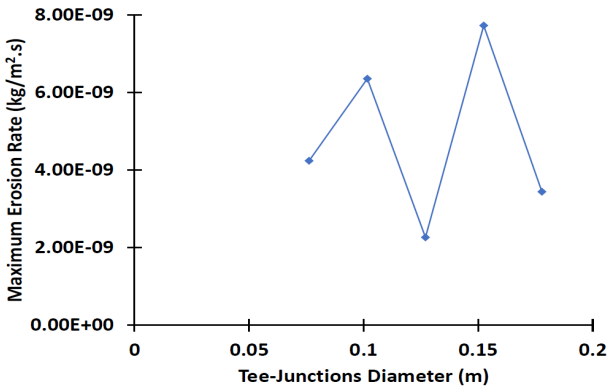

Figure 18. Maximum erosion rate (kg/m^2.s) versus tee-junctions diameter (m)

4. CONCLUSION

The tee junctions in light crude oil ($C_{19}H_{30}$)-solid (sand) flow were simulated under three different flow conditions which are the particles size, stream velocity, and tee-junctions diameter using the CFD software. Based on the work done, it can be deduced that the maximum erosion rate in the tee-junctions is influenced by particles size and stream velocity. The maximum erosion rate was significantly decreased (almost 86% reduction) when the size of particles is changed from 100 µm to 500 µm. On the other side, the changes of stream velocity from 3 m/s to 7 m/s cause in tremendously increased (almost 133% increment) in maximum erosion rate. However, there is no correlation found for the maximum erosion rate (increased or decreased) with the tee-junctions diameter as it involved large particle size of sand (200 µm). The simulation results possibly will able to assist in design process for the real field application which possess the same condition and parameters. By having a proper design, the erosion rate in tee-junctions could be minimized and hence, reduce the cost of maintenance in terms of tee-junctions replacement.

ACKNOWLEDGEMENT

The Department of Energy Engineering, School of Chemical and Energy Engineering and UTM are highly acknowledged for providing continuous technical and facilities support.

REFERENCES

[1] I. U. Toor, H. M. Irshad, H. M. Badr and M. A. Samad, The effect of impingement velocity and angle variation on the erosion corrosion performance of API 5L-X65 carbon steel in a flow loop, *Metals*, 8, 2018, 402.

[2] A. Mansouri, *A combined CFD-experimental method for developing an erosion equation for both gas-sand and liquid-sand flows*, PhD Thesis, The University of Tulsa, 2016.

[3] G. Ou, K. Bie, Z. Zheng, G. Shu, C. Wang and B. Cheng, Numerical simulation on the erosion wear of a multiphase flow pipeline, *The International Journal of Advanced Manufacturing Technology*, 96, 2018, 1705-1713.

[4] M. Parsi, K. Najmi, F. Najafifard, S. Hassani, B. S. McLaury and S. A. Shirazi, A comprehensive review of solid particle erosion modeling for oil and gas wells and pipelines applications, *Journal of Natural Gas Science and Engineering*, 21, 2014, 850-873.

[5] X. Chen, B. S. McLaury and S. A. Shirazi, Numerical and experimental investigation of the relative erosion severity between plugged tees and elbows in dilute gas/solid two-phase flow, *Wear*, 261, 2006, 715-729.
[6] D. Vigolo, I. M. Griffiths, S. Radl and H. A. Stone, An experimental and theoretical investigation of particle–wall impacts in a T-junction, *Journal of Fluid Mechanics*, 727, 2013, 236-255.
[7] J. Zhang, Y. Bai, J. Kang and X. Wu, Failure analysis and erosion prediction of tee junction in fracturing operation, *Journal of Loss Prevention in the Process Industries*, 46, 2017, 94-107.
[8] G. J. Brown, Erosion prediction in slurry pipeline tee-junctions, *Applied Mathematical Modelling*, 26, 2002, 155-170.
[9] Y. Doroshenko, J. Doroshenko, V. Zapukhliak, L. Poberezhny and P. Maruschak, Modeling computational fluid dynamics of multiphase flows in elbow and T-junction of the main gas pipeline, *Transport*, 34, 2019, 19-29.
[10] X. Chen, B. S. McLaury and S. A. Shirazi, Application and experimental validation of a computational fluid dynamics (CFD)-based erosion prediction model in elbows and plugged tees, *Computers & Fluids*, 33, 2004, 1251-1272.
[11] A. Farokhipour, Z. Mansoori, A. Rasteh, M. A. Rasoulian, M. Saffar-Avval and G. Ahmadi, Study of erosion prediction of turbulent gas-solid flow in plugged tees via CFD-DEM, *Powder Technology*, 352, 2019, 136-150.
[12] R. Verma, V. Agarwal, R. Pandey and P. Gupta, Erosive wear reduction for safe and reliable pneumatic conveying systems: review and future directions, *Life Cycle Reliability and Safety Engineering*, 7, 2018, 193-214.
[13] H. Pouraria, J. K. Seo and J. K. Paik, Numerical study of erosion in critical components of subsea pipeline: Tees vs bends, *Ships and Offshore Structures*, 12, 2017, 233-243.
[14] M. A. H. Yusof, Z. Zakaria, A. Supee and M. Z. M. Yusop, Prediction of erosion rate in elbows for liquid-solid flow via computational fluid dynamics (CFD), *Applications of Modelling and Simulation*, 3, 2019, 28-38.
[15] C. A. R. Duarte, F. J. de Souza and V. F. dos Santos, Numerical investigation of mass loading effects on elbow erosion, *Powder Technology*, 283, 2015, 593-606.
[16] R. E. Vieira, A. Mansouri, B. S. McLaury and S. A. Shirazi, Experimental and computational study of erosion in elbows due to sand particles in air flow, *Powder Technology*, 288, 2016, 339-353.
[17] M. A. Habib, H. M. Badr, R. Ben-Mansour and M. E. Kabir, Erosion rate correlations of a pipe protruded in an abrupt pipe contraction, *International Journal of Impact Engineering*, 34, 2007, 1350-1369.
[18] M. Cable, An evaluation of turbulence models for the numerical study of forced and natural convective flow in Atria, *Department of Mechanical and Materials Engineering*, Queen's University, Ontario, Canada, 2009.
[19] T.-H. Shih, W. W. Liou, A. Shabbir, Z. Yang and J. Zhu, A new k-ϵ eddy viscosity model for high reynolds number turbulent flows, *Computers & Fluids*, 24, 1995, 227-238.
[20] F. Durst, D. Miloievic and B. Schönung, Eulerian and Lagrangian predictions of particulate two-phase flows: a numerical study, *Applied Mathematical Modelling*, 8, 1984, 101-115.
[21] A. Picart, A. Berlemont and G. Gouesbet, Modelling and predicting turbulence fields and the dispersion of discrete particles transported by turbulent flows, *International Journal of Multiphase Flow*, 12, 1986, 237-261.
[22] Q. Q. Lu, J. R. Fontaine and G. Aubertin, A lagrangian model for solid particles in turbulent flows, *International Journal of Multiphase Flow*, 19, 1993, 347-367.
[23] R. Clift, J. R. Grace and M. E. Weber, *Bubbles, drops, and particles*, Dover Publications, Inc., Mineola, New York, 2005.
[24] J. E. Miller, *Slurry Erosion: Uses, Applications, and Test Methods: a Symposium*, ASTM International, 1987.
[25] N. Barton, Erosion in elbows in hydrocarbon production systems: Review document, *TÜV NEL Limited, Research Report*, 115, 2003.

APPENDIX

Nomenclature	
x	space coordinate
$\bar{U}$	time average velocity component
P	pressure
u	fluctuating component of velocity
k	kinetic energy of turbulence
$C_{\mu}, C_{\varepsilon 1}, C_{\varepsilon 2}$	empirical constants in k-epsilon turbulence model
G_k	production of turbulent kinetic energy due to mean velocity gradients
F	force
m	mass
V	velocity
C_D	drag coefficient
Re_f	fluid Reynolds number
Re_s	particle relative Reynolds number
t	time
g	gravity
$\dot{m}$	mass flow rate
ER	erosion rate
$C(\phi)$	function of the diameter
$f(\alpha)$	function of the impact angle
V	relative velocity
A	area
t	time
Superscripts	
___	time average
.	time rate
b(V)	function of relative velocity

Greek symbols	
ρ	density
μ	viscosity
δ_{ji}	Kronecker delta
σ_k	effective Prandtl number for k
σ_{ε}	effective Prandtl number for ε
ε	rate of dissipation of the kinetic energy
ϕ	diameter
∂	partial derivative
Subscripts	
i, j, k	spatial coordinate indices
f	fluid
T	turbulence
eff	effective
D	drag
P	pressure gradient
B	buoyancy
A	added mass
p	particle
$face$	wall face where the particles strikes the boundary